MyoD family inhibitor proteins act as auxiliary subunits of PIEZO channels

Zijing Zhou[1,2*], Xiaonuo Ma [3*], Yiechang Lin[4], Delfine Cheng[1,2], Navid Bavi[5], Genevieve A. Secker[6], Jinyuan Vero Li[1,2], Vaibhao Janbandhu[1,2], Drew L. Sutton[6,7], Hamish S. Scott[6,7,8], Mingxi Yao[9], Richard P Harvey[1,2], Natasha L. Harvey[6,7], Ben Corry[4], Yixiao Zhang[3#] & Charles D Cox[1,10#]

[1]Victor Chang Cardiac Research Institute, Sydney, NSW, 2010, Australia. [2] School of Clinical Medicine, Faculty of Medicine and Health, University of New South Wales, Sydney, NSW 2052, Australia. [3]Interdisciplinary Research Center on Biology and Chemistry, Shanghai Institute of Organic Chemistry, Chinese Academy of Sciences, China. [4]Research School of Biology, Australian National University, Acton, ACT 2601, Australia. [5]Department of Biochemistry and Molecular Biophysics, University of Chicago, Chicago, IL 60637, USA. [6]Centre for Cancer Biology, University of South Australia and SA Pathology, Adelaide 5001, Australia. [7]Adelaide Medical School, University of Adelaide, Adelaide, 5005 Australia. [8]Department of Genetics and Molecular Pathology, SA Pathology, Adelaide 5000, Australia. [9]Department of Biomedical Engineering, Southern University of Science and Technology, Shenzhen 518055, China. [10]School of Biomedical Sciences, Faculty of Medicine & Health, UNSW Sydney, Kensington, NSW, 2052, Australia

*These authors contributed equally

#Corresponding authors:

E-mail: c.cox@victorchang.edu.au or yzhang@mail.sioc.ac.cn

Abstract

PIEZO channels are critical cellular sensors of mechanical forces. Despite their large size, ubiquitous expression, and irreplaceable roles in an ever-growing list of physiological processes, few bona fide PIEZO channel binding partners have emerged. Here we identify MyoD family inhibitor proteins (MDFIC and MDFI), as a novel family of PIEZO1/2 interacting partners. These transcriptional regulators, bind to PIEZO1/2 channels potently regulating channel inactivation. Using single-particle cryo-electron microscopy we map the interaction site in MDFIC to a lipidated, C-terminal helix that inserts laterally into the PIEZO1 pore module. This novel family of PIEZO interacting proteins fit all the criteria for auxiliary subunits, explain the vastly different gating kinetics of endogenous PIEZO channels observed in many cell types and illuminate new mechanisms underlying human lymphatic vascular disease.

Main

Mechanical forces govern life forms at every level of complexity. To decode mechanical cues cells are endowed with a palette of molecular force sensors. Among these sensors, ion channels form a structurally diverse superfamily involved in a wide array of physiological processes (*1*). In particular, PIEZO channels (*2*) have emerged as force sensors critical in determining how cells sense their physical environment (*3*).

PIEZO channels assemble as trimers, where the arms of individual monomers extend out laterally in the membrane from a central ion conducting pore module (*4-6*). This molecular assembly possesses all the structural requirements for mechanosensitivity (*7, 8*). However, PIEZO channels can display non-uniform sub-cellular localization (*9-12*) and exhibit different gating kinetics (principally slower inactivation (*2, 13-18*)) in many cell types when compared to heterologous expression systems. These observations could have many molecular explanations; differences in lipid composition (*17, 19*), curvature dependent sorting (*9, 12*), or protein-protein interactions. Many ion channels interact with auxiliary subunits (*20, 21*) to modify their cellular location and gating properties. Despite significant effort, no bona fide families of PIEZO channel binding partners have emerged.

Here, using affinity capture mass spectrometry (AC-MS), we identify a new family of PIEZO channel interacting molecules, namely the MyoD family inhibitor proteins MDFIC and MDFI. We map out the functional consequences of this interaction for PIEZO1/2 and provide the structural basis of the interaction using single-particle cryo-electron microscopy (cryo-EM). Our structural and functional data not only reveal a novel auxiliary subunit of PIEZO channels but may reveal a putative conserved binding site for other membrane associated proteins that modulate PIEZO channel function. As MDFIC and PIEZO1 are linked to lymphatic vascular disease these findings may also uncover novel disease mechanisms and enable the development of new PIEZO-targeted therapeutic modalities.

Novel PIEZO channel binding proteins

To identify new binding partners for PIEZO channels we utilized two complementary AC-MS strategies in conjunction with two CRISPR/cas9 edited PIEZO1 human dermal fibroblast (hDF) lines (**Fig. 1A-F; fig. S1**). We utilized fibroblasts as PIEZO1 expressed in fibroblasts from numerous tissue origins exhibit slower inactivation kinetics (*16, 18, 22*). Our pipeline consisted of three comparator groups; 1) hDF with PIEZO1 ablated using CRISPR/cas9 compared to wild-type cells where PIEZO1 was enriched through a conventional anti-PIEZO1 antibody strategy, 2) hDF with a HaloTag knocked in to the endogenous PIEZO1 loci (P1-Halo) where PIEZO1 was enriched using HaloTrap resin, and 3) primary human cardiac fibroblasts (hCF) where PIEZO1 was enriched through a conventional anti-PIEZO1 antibody strategy. We then stringently analyzed the resulting mass spectrometry data to identify PIEZO1 interacting proteins present in all 3 groups that did not present in any of their respective negative controls. Using these criteria only two proteins were identified, the first of which was PIEZO1 (**Fig. 1E**). This provided strong validation for both affinity capture strategies. The second was the sparsely studied transcriptional regulator MDFIC (MyoD family inhibitor domain containing protein (*23, 24*)). Mass spectrometry provided 39 ± 14 % coverage of MDFIC averaged over the 3 groups (**Fig. 1F**).

First, using RNA expression data we identified many cell types, in addition to fibroblasts, that co-express PIEZO channels and the MyoD family inhibitor proteins, MDFIC or MDFI (**fig. S2A-B**)(*25*). We then validated the interaction by expressing N-terminally HA-tagged MDFIC with PIEZO1 in HEK293T cells. We could reciprocally capture PIEZO1 with MDFIC and the complex was present under mechanical (shear stress) or chemical activation (10 μM Yoda-1(*26*)) of PIEZO1 (**fig. S2C**), indicating the stability of the interaction. We also confirmed PIEZO1 interacted with the closely related MDFI (*27*) (**fig. S2D**). We next confirmed that MDFIC selectively interacted with PIEZO1/2 channels using native gels, identifying MDFIC at the size of the respective PIEZO1/2 trimers but not in oligomeric complexes of TRPM4 or TREK-1 (**fig. S2E**). In doing so we noticed that co-expression with PIEZO1 enhanced the protein levels of both MDFIC and MDFI (>3-4 fold; **fig. S2C-E**). To probe the specificity of this effect we co-expressed MDFIC with PIEZO1 and PIEZO2 and compared the MDFIC levels when expressed alongside other ion channels. Co-expression of MDFIC with GFP alone, TRPM4, TRPV4 or TREK-1 did not have the same influence (**fig. S3A-B**). Treating cells expressing MDFIC only or MDFIC and PIEZO1 with cycloheximide illustrated that this increase in MDFIC protein level was due to decreased MDFIC turnover, meaning the complex is stabilizing MDFIC (**supplementary text and fig. S3C-D**).

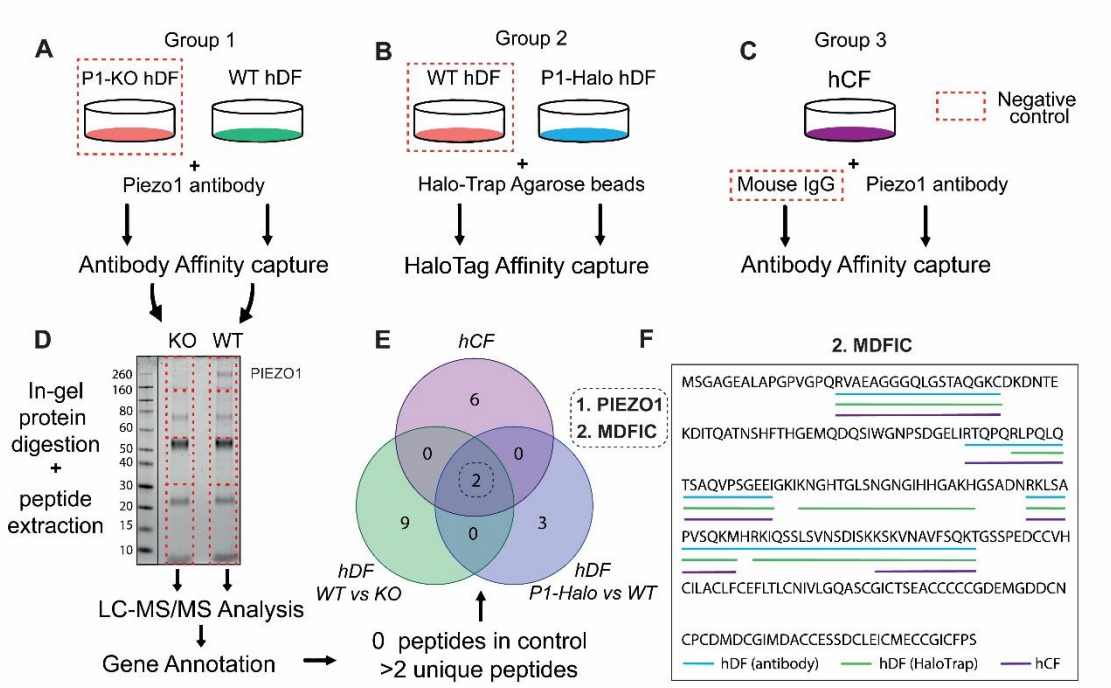

Figure 1 Affinity capture mass spectrometry (AC-MS) identifies a new family of PIEZO channel binding partners.

*Groups for AC-MS consisted of; (**A**) wild-type (WT) and PIEZO1 knockout (KO) human dermal fibroblasts (hDF; n=2), (**B**) WT and PIEZO1-HaloTag (P1-Halo) knockin hDF (n=2), **(C)** primary human cardiac fibroblasts (hCF; n=2). **(D)** Affinity captured protein lysates were run on SDS-Page gels and sectioned into quadrants (red dashed lines). Each quadrant was subjected to in-gel protein digestion followed by peptide extraction and liquid chromatography (LC) followed by mass spectrometry (MS). **(E)** Venn diagram illustrating proteins identified in each experimental group that had ≥2 unique peptides which were absent from negative control replicates. (**F**) Two proteins were identified in all positive control replicates, PIEZO1 and MyoD Family Inhibitor domain Containing protein, MDFIC. Alignment of unique MDFIC peptides identified by MS.*

MDFIC binds the PIEZO1 pore module

To provide molecular detail of the interaction we co-expressed mouse PIEZO1 with N-terminally FLAG-tagged mouse MDFIC and purified the complex using FLAG resin. Using single-particle cryo-EM, we determined the structure of the PIEZO1-MDFIC complex at an overall resolution of 3.66 Å (**Fig. 2A-B; fig. S4**). We resolved the C-terminal 21 amino acids of MDFIC (**Fig. 2A-D**) while the N-terminal portion displayed little or no density, presumably due to local dynamics. The resolved region of MDFIC (residues 225-246) consists of an amphipathic helix that sits parallel to the membrane at the membrane interface (**Fig. 2C**). This helix inserts laterally into the PIEZO1 pore module, nestling between the anchor domain and the outer helix of PIEZO1 (**Fig. 2C-D**) making significant contacts with His2116, Phe2010, and

Gln2123 from the α1 helix of the anchor domain, Val2187, Met2191, and Leu2195 from the outer helix and Phe2484 and Phe2485 at the base of the inner helix that lines the PIEZO1 pore (**Fig. 2E**). The amphipathic helix of MDFIC consists of a sequence of five cysteines that point towards the bilayer interior (**Fig. 2E-F**) and a sequence of four negatively charged residues that point towards the solvent, forming salt bridges with multiple lysine residues (**Fig. 2F-G**). The MDFIC C-terminus penetrates far enough that it comes close to the cytoplasmic constriction formed by Met2493/Phe2494 (**Fig. 2H**) and residues critical for voltage-dependent inactivation (Lys2479/Arg2482)(*28, 29*). Despite its central location MDFIC binding did not noticeably influence the closed structure of the PIEZO1 pore module (**fig. S4I)**.

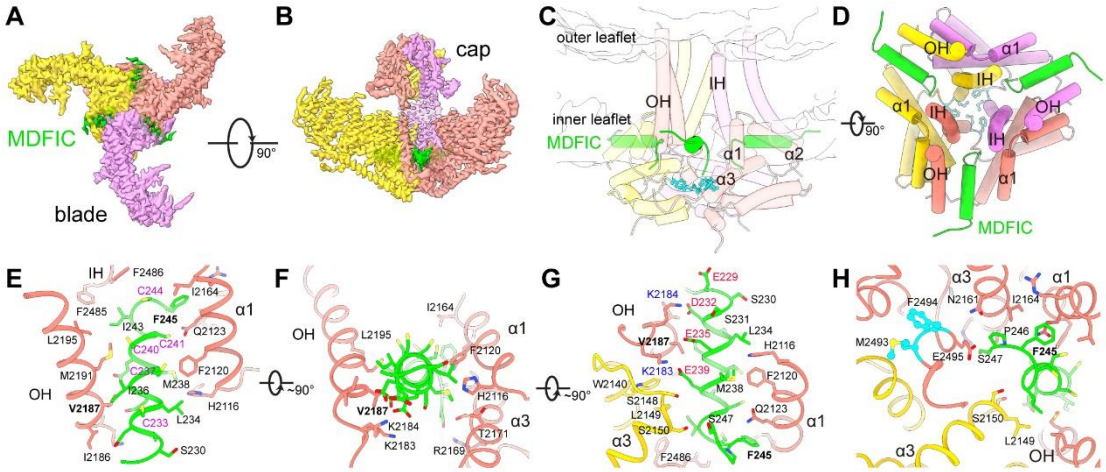

Figure 2 Structural elucidation of the PIEZO1-MDFIC complex.

(A-B) *Cryo-EM density maps of the mouse PIEZO1-MDFIC complex at 3.66 Å nominal resolution viewed from the top (**A**) and side (**B**) with the resolved MDFIC region coloured green. (**C**) The distal C-terminal of MDFIC resides parallel to the bilayer between the anchor domain (α1- α3) and the outer helix (OH). The cytoplasmic constriction residues Met2493 and Phe2494 are shown in cyan. (**D**) The C-terminal region of MDFIC protrudes deep into the pore module of PIEZO1 approaching the inner helix (IH). (**E-G**) The interactions between PIEZO1 and MDFIC shown in membrane facing view (**E**), lateral view (**F**) and cytoplasmic facing view (**G-H**). Variants linked to lymphatic malformations (mPIEZO1 V2187 and mMDFIC F245) are labelled bold.*

As both PIEZO1 and MDFIC are essential for lymphatic development in mice and humans (*24, 30, 31*) we investigated, using the ClinVar database, whether any disease-causing mutations were located within this binding interface. We found a mutation in both PIEZO1 (**Fig. 2E,G**; human V2171F) and MDFIC (**Fig. 2E,H**; human F244L) associated with human lymphatic disease.

MDFIC and MDFI regulate PIEZO gating

Given the location of MDFIC binding we next tested whether human MDFIC and MDFI modified human PIEZO1 (hPIEZO1) gating. MDFIC and MDFI expressed alone did not generate stretch activated currents (**fig. S5A-D**). Compared with hPIEZO1 alone, co-expression with MDFIC or MDFI resulted in a mild right-shift in the pressure response curve, a marked increase in the peak stretch-evoked currents, a significant slowing of channel inactivation and continued channel gating even after the pressure was released (**Fig. 3A-H; fig. S5**). We quantified the latter of these effects using the current remaining 1 second post application of stretch (I_{post}). MDFIC did not influence PIEZO1 protein levels but did increase PIEZO1 single channel conductance (**supplemental text and fig. S6**). Thus, the increase in stretch-activated currents in the presence of MDFIC is likely driven by changes in conductance and its strong effect on inactivation. The slow 'closure' after pressure release (signified by increased I_{post}) was more pronounced at hyperpolarizing voltages suggesting an effect on the structural transition governing voltage-dependent inactivation (*28, 29*) (**fig. S7A-B**). Consistent with this the channel could be rapidly closed by flipping the voltage to depolarizing potentials (**fig. S7C-D**). We identified slower inactivation in both cell-attached and whole-cell modes (**fig. S8**).

Importantly, MDFIC expression did not influence the function of mechanosensitive TREK-1 channels ruling out non-specific effects (**fig. S9**). Given the C-terminus of MDFIC is resolved in the structure and is highly homologous in MDFI (whereas the N-termini of MDFIC and MDFI bear little resemblance and have no known function) we asked whether the MyoD inhibitor domain of MDFIC (amino acid 165-246 - C-81) expressed alone could modify PIEZO1 function. Indeed, despite being unstable this domain reduces channel inactivation (**Fig. 3D,G**). Moreover, the C-81 protein could bind to PIEZO1 with its levels being dramatically increased by PIEZO1 co-expression (**fig. S10A-C**). Conversely, truncation of the C-terminal 20 residues (ΔC20) prevented MDFIC from regulating PIEZO1 gating (**Fig. 3E-G**). This truncation reduced the interaction with PIEZO1, and its protein levels were not significantly increased by PIEZO1 (**fig. S10C-E**). Thus, the observed increase in MDFIC levels was dependent on the direct PIEZO1-MDFIC interaction and MDFIC's distal C-terminus strongly influences its stability.

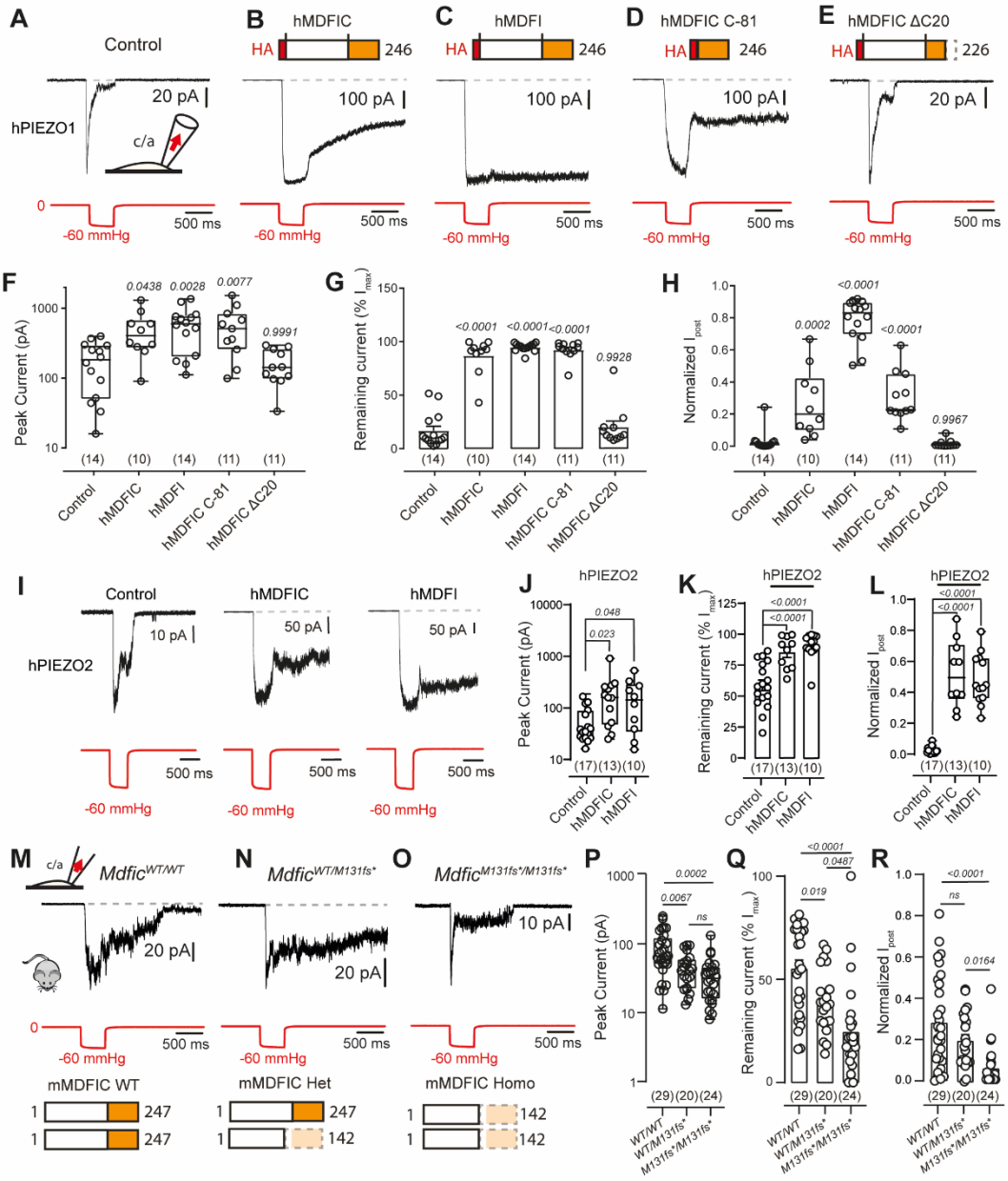

Figure 3 MyoD family inhibitor proteins regulate PIEZO1 and PIEZO2 channel gating.
*(**A to E**) Representative cell-attached (c/a) patch-clamp recordings from hPIEZO1 control and in the presence of hMDFIC, hMDFI, the conserved C-terminus of MDFIC (hMDFIC C-81) and with MDFIC lacking its C-terminal 20 amino acids (hMDFIC ΔC20) at a holding potential of -65mV. (**F to H**) Quantification of peak currents per patch, % current remaining and normalized current 1 second after pressure was released (Normalized I_{post}) for replicates of cell-attached recordings shown in A-E. **(I to L)** Representative cell-attached recordings from human PIEZO2 (PIEZO2) control and in the presence of hMDFIC and hMDFI and quantification of replicates. **(M to O)** Representative cell-attached (c/a) patch-clamp recordings from mouse cardiac fibroblasts isolated at E16.5 from WT, heterozygous and homozygous $Mdfic^{M131fs*}$ mice. **(P to R)** Quantification of peak current per patch, % current remaining and normalized I_{post} for*

replicates of cell-attached recordings shown in m-o (All data displayed as mean ± SEM or as maximum to minimum box and whiskers plot; p-values determined using one-way ANOVA and Tukey's multiple comparison).

Given the homology of PIEZO1 and PIEZO2 in this region we additionally showed that the same regulation occurs for both human PIEZO2 and mouse PIEZO orthologues (**Fig. 3I-L; fig. S11**). Moreover, the expression of MDFIC and MDFI correlated with the native inactivating phenotype of PIEZO1 in multiple human and mouse cell types (**fig. S12**). However, we wanted to know if the loss of MDFIC could modify the kinetics of native PIEZO1 currents. To answer this, we utilized a mouse model of a recurrent MDFIC variant found in patients with the complex lymphatic anomaly known as central conducting lymphatic anomaly (*24*). This truncating variant lacks the complete conserved C-terminal region but retains the N-terminal region (*24*). Assessment of PIEZO1 activity in embryonic cardiac fibroblasts isolated from E16.5 wild-type (WT/WT), heterozygous (WT/M131fs*) and homozygous mice (M131fs*/M131fs*), revealed that fibroblasts from mice harboring C-terminally truncated MDFIC had PIEZO1 currents which were smaller and inactivated more rapidly (**Fig. 3M-R)**. This effect on inactivation was phenocopied by knocking down MDFIC using siRNA **(supplemental text and fig. S13**).

PIEZO1 regulation requires MDFIC lipidation

Cryo-EM maps of MDFIC revealed extra densities on Cys233, 237, 240, 241 and 244 (**Fig. 4A**). Given this helix is situated at the membrane interface and contains motifs for cysteine lipidation (*32*) we hypothesized these extra densities resulted from lipidation, the covalent addition of acyl chains to amino acids (*33*). A second cryo-EM complex of the MDFIC mutant Cys240Ala at 3.59 Å selectively removed extra density from Cys240 consistent with post translational modification (**fig. S14**). Acyl biotin exchange confirmed that MDFIC was palmitoylated (**Fig. 4B**). Using mass tagging with PEGylated maleimide (increases mass per palmitoylated site) we show there are at least 3 sites for lipidation on MDFIC (**Fig. 4C**), that two are in the distal C-terminus (**supplemental text and fig. S15**) and that like most lipidated proteins MDFIC associates with the plasma membrane (**Fig. 4D**).

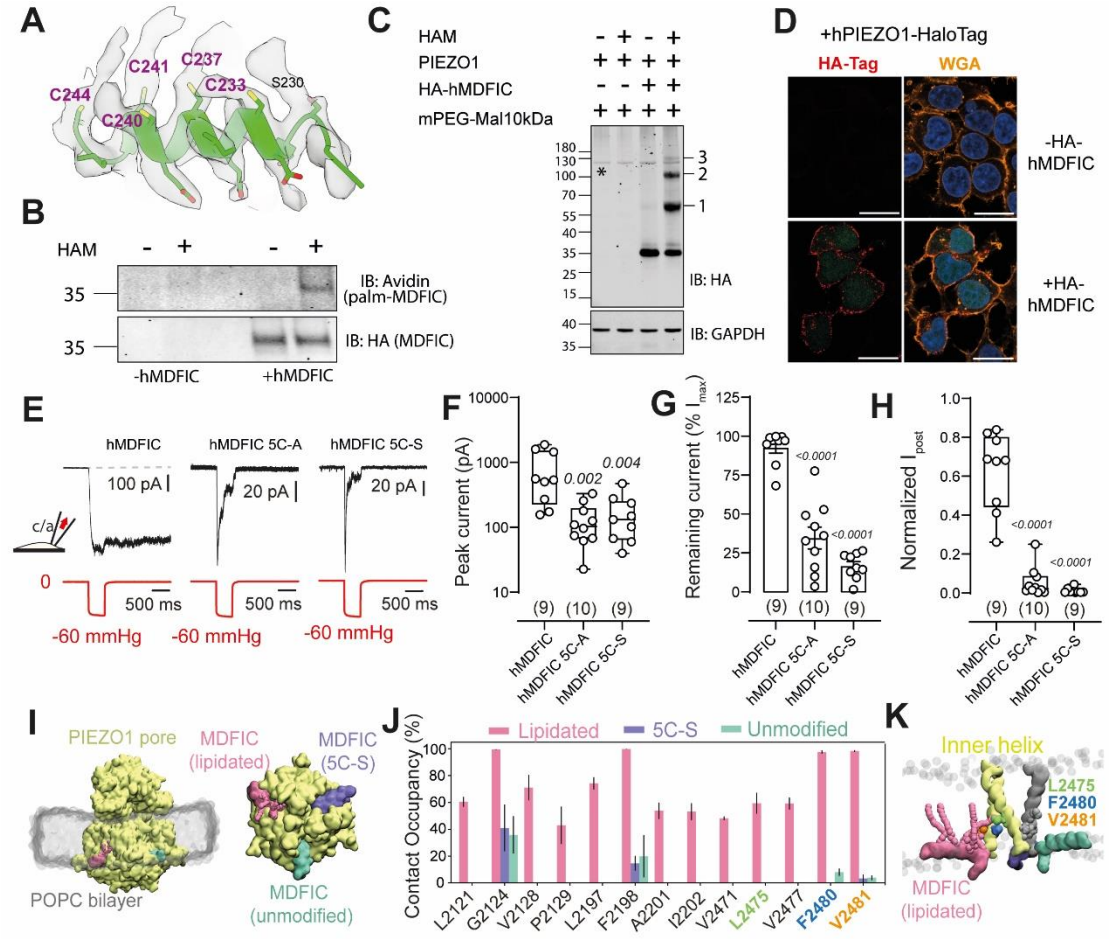

Figure 4 C-terminal lipidation of MDFIC underlies regulation of PIEZO1 channel gating. ***(A)*** *Cryo-EM density map showing extension of density on cysteine residues within the C-terminus of MDFIC.* ***(B)*** *Representative immunoblot (IB) using Avidin (top) or anti-HA (bottom) from acyl biotin exchange showing lysate +/- hydroxylamine (HAM). Blots show a band at the correct size for HA-MDFIC but the biotinylated MDFIC can only be seen in the HAM treated group indicating palmitoylated-MDFIC (palm-MDFIC).* ***(C)*** *Mass-tagging of MDFIC using mPEGylated maleimide reveals at least 3 palmitoylation sites labelled 1-3 (* represents non-specific band in all groups).* ***(D)*** *Membrane localized HA-MDFIC in HEK293T cells, membrane delineated using wheatgerm agglutinin (WGA).* ***(E)*** *Representative cell-attached recordings of hPIEZO1 in the presence of wild-type MDFIC and mutation of the 5 C-terminal cysteine residues to either alanine (5C-A) or serine (5C-S) abolishes the regulatory effects of MDFIC.* ***(F-H)*** *Quantification of peak currents per patch, % current remaining and normalized I_{post} for replicate recordings of panel E.* ***(I)*** *All-atom molecular dynamic simulations of the mPIEZO1 pore module in complex with unmodified (green), 5C-S mutant (purple) and lipidated MDFIC (pink) C-termini.* ***(J-K)*** *The lipidated MDFIC acyl chains interact selectively with inner helix residues critical for PIEZO1 channel inactivation. (p-value determined using one-way ANOVA and Tukey's multiple comparison).*

To check if MDFIC lipidation was functionally relevant we mutated all five C-terminal cysteines to alanine or serine. Expression of MDFIC with Cys233/237/240/241/244Ala (5C-A) or Cys233/237/240/241/244Ser (5C-S) did bind to PIEZO1 but neither mutant influenced PIEZO1 activity suggesting that the lipidation of the MDFIC C-terminus is critical for PIEZO1 regulation (**Fig. 4F-H; fig. S15C**).

To probe the role of lipidation we utilized all-atom molecular dynamics simulations of the PIEZO1 pore module (1956-2547) in complex with the MDFIC C-terminus (**Fig. 4I-K; fig. S16**). Simulations consisted of 3 MDFIC monomers; one unmodified, one lipidated at all 5 cysteine residues in the helix and one where each cysteine was mutated to serine (**Fig 4I**). All variations of the MDFIC C-terminus remained stably bound (**fig. S16A-B**). Overlay of a snapshot from simulations shows the acyl chains coincide with the additional MDFIC cryo-EM densities (**fig. S16C**). We compared all interactions occurring in either unmodified or lipidated monomers to those in the 5C-S mutant that we know binds but does not modulate function (**Fig 4J; fig. S16**). Interactions between the unmodified and 5C-S MDFIC were indistinguishable, supporting the importance of MDFIC lipidation in modulating PIEZO1 function. In contrast, the lipidated MDFIC had multiple unique interactions with inner helix residues (**Fig 4J-K; fig. S16D-E**). Some of these residues within the inner helix are critical for inactivation including Leu2475 (*34*) making this the likely pathway for functional modification. Given MDFIC would need to stay bound throughout the PIEZO1 conformational cycle we also examined if MDFIC could bind to the flattened state of PIEZO1 (*35*). When MDFIC is aligned to the same pocket simulations show it interacts with the inner helix and remains stably bound (**fig. S16F-H**).

Discussion

PIEZO channels act as critical transducers of physical forces. In many primary cell types they show non-uniform subcellular localization (*9-11*) and gating kinetics that look dissimilar to heterologously expressed channels (e.g. slower inactivation (*13, 16*)). This includes currents reported in the original PIEZO channel discovery article from C2C12 cells that slowly inactivated (*2*). Several possible explanations for this behavior have been posited. In endothelial cells, the lipid ceramide has been proposed as a potent regulator of inactivation (*17*). In fact, various different lipid types can regulate PIEZO channel gating (*19, 36*) and may even provide a mechanism to treat PIEZO-related pathologies (*37*). In other ion channel families, gating regulators also take the form of auxiliary subunits (*20*). Using affinity capture mass spectrometry we identified a new family of PIEZO channel binding partners, the MyoD family inhibitor proteins MDFI and MDFIC. These proteins bind to the PIEZO1 pore module via their conserved C-terminus, regulating channel inactivation. MyoD family inhibitor domain proteins fit all the criteria for auxiliary subunits; 1) they are non-pore-forming subunits, 2) they have a direct and stable interaction with a pore-forming subunit, 3) they modulate channel properties in heterologous systems, 4) they regulate channel activity at endogenous levels in native cells

(*21*). This regulation of PIEZO channel inactivation critically involves palmitoylation of the C-terminal of MDFIC. As palmitoylation is a reversible lipid addition (*33*) this adds the intriguing potential for dynamic spatio-temporal regulation of PIEZO inactivation by MDFIC. While our 'fibroblast-centric' screen identified few other PIEZO channel binding partner candidates, we speculate the binding region of MDFIC could form a conserved binding site for other membrane associated PIEZO regulators. In support of this, the PIEZO1 lysine residues that form salt bridges with MDFIC have been proposed to interact with other proteins (*38*). While PIEZO1 channels can function as independent mechanosensors in simplified systems ample evidence suggests that PIEZOs, particularly PIEZO2, may receive force through molecular tethers (*39*). Given the location of binding it remains possible that MDFIC could act as a tethering molecule.

An important question is how ubiquitous is this regulatory mechanism? MDFIC and MDFI are absent from many cell types with rapidly inactivating PIEZO1 channels including LNCaP (*15*) and N2A (*2*) but are expressed in others including fibroblasts (*16, 18, 22*) and endothelial cells that exhibit slowly inactivating PIEZO1 currents (*13-15, 18*). Indeed, we isolated cardiac fibroblasts from mice harbouring a truncated MDFIC lacking its C-terminus (*24*) where PIEZO1 exhibited faster inactivation than WT fibroblasts. Thus, MDFIC/MDFI mediated regulation of PIEZO channels could be widely utilized. The similar lymphatic phenotypes associated with loss of function of MDFIC (*24*) and PIEZO1 (*30, 31*) means this mechanism may unearth new molecular aspects associated with lymphatic vascular disease. Furthermore, both MDFIC and MDFI bind to transcription factors (*24, 40*) (including GATA2 a master regulator of lymphatic valve development (*41*)). Whether PIEZO1/2 influence this aspect of their function is unknown but may set the stage towards the unveiling of a direct mechano-signaling pathway via PIEZOs to transcription, through GATA2 or other transcription factors.

In summary we describe the discovery of a new family of PIEZO channel binding proteins and report, to our knowledge, the first structural complex of PIEZO1 with any binding partner. We propose that this family of molecules, which according to all criteria seem to act as cell-type specific auxiliary subunits of PIEZO channels, provides a new frontier in mechanobiology.

Acknowledgements

We thank Drs Boris Martinac, Eduardo Perozo and Jie Xu for useful scientific discussions and critical reading of the manuscript. We thank the Cryo-EM center at the Interdisciplinary Research Center on Biology and Chemistry, Shanghai Institute of Organic Chemistry for help with data collection.

Funding: CDC is supported by an Australian Research Council (ARC) Future Fellowship (FT220100159). YZ is supported by STI2030-Major Projects (7400), Shanghai Municipal of Science and Technology Project (20JC1419500) and Shanghai Municipal Science and

Technology Major Project (2019SHZDZX02). BC acknowledges ARC funding (DP200100860). This research was undertaken with the assistance of resources and services from the National Computational Infrastructure, supported by the Australian Government. The mouse model was supported by Medical Research Future Fund, Genomics Health Futures Mission grant GHFM76777.

Author Contributions: Z.Z, M.Y and D.C. generated cell lines and performed biochemical and imaging experiments. Z.Z, N.B. and C.D.C performed electrophysiology. G.A.S, D.L.S, H.S, V.J, R.P.H and N.L.H generated animal models and isolated cells. Z.Z and J.V.L generated reagents. X.M. and Y.Z. performed cryo-EM structural studies. B.C and Y.L. performed MD simulations. C.D.C and Y.Z. conceived and supervised the project. All authors wrote and approved the manuscript.

Competing interests: The authors declare no competing interests.

Data availability: The composite map of the PIEZO1-MDFIC complex has been deposited in the Electron Microscopy Data Bank under the accession codes EMD-35577. The atomic coordinates have been deposited in the Protein Data Bank under the accession codes 8IMZ. The composite map may contain artificial features near the boundaries of the masks. The consensus map, masked refined cap map, masked refined TMD map, and the map of PIEZO1-MDFIC (C240) have been deposited under the accession codes EMD-36241, EMD-36242, EMD-36243, and EMD-36244. All data are available in the main text or the supplementary materials.

(*42, 43*) **(*44*) (*45*) (*46*).(*35*) (*47*)**, **(*48*) (*49*)** (*50*) (*32*) (*51*) (*35*) (*52*) (*53, 54*) (*55, 56*) (*57*) (*58*) (*59, 60*) (*61*) (*62*)

References

1. J. M. Kefauver, A. B. Ward, A. Patapoutian, *Nature* **587**, 567-576 (2020).
2. B. Coste *et al.*, *Science* **330**, 55-60 (2010).
3. S. E. Murthy, A. E. Dubin, A. Patapoutian, *Nat Rev Mol Cell Biol* **18**, 771-783 (2017).
4. K. Saotome *et al.*, *Nature* **554**, 481-486 (2018).
5. Q. Zhao *et al.*, *Nature* **554**, 487-492 (2018).
6. Y. R. Guo, R. MacKinnon, *Elife* **6**, (2017).
7. C. D. Cox *et al.*, *Nat Commun* **7**, 10366 (2016).
8. R. Syeda *et al.*, *Cell Reports* **17**, 1739-1746 (2016).
9. S. Yang *et al.*, *Nature Communications* **13**, 7467 (2022).

10. J. R. Holt *et al.*, *eLife* **10**, e65415 (2021).
11. M. Yao *et al.*, *Sci Adv* **8**, eabo1461 (2022).
12. G. Vaisey, P. Banerjee, A. J. North, C. A. Haselwandter, R. MacKinnon, *eLife* **11**, e82621 (2022).
13. S. Wang *et al.*, *Nature Communications* **11**, 2303 (2020).
14. J. I. del Mármol, K. K. Touhara, G. Croft, R. MacKinnon, *eLife* **7**, e33149 (2018).
15. R. Maroto, A. Kurosky, O. P. Hamill, *Channels (Austin)* **6**, 290-307 (2012).
16. E. Glogowska *et al.*, *Cell Rep* **37**, 110070 (2021).
17. J. Shi *et al.*, *Cell Rep* **33**, 108225 (2020).
18. N. M. Blythe *et al.*, *J Biol Chem* **294**, 17395-17408 (2019).
19. L. O. Romero *et al.*, *Nat Commun* **10**, 1200 (2019).
20. A. C. Dolphin, *The Journal of Physiology* **594**, 5369-5390 (2016).
21. D. Yan, S. Tomita, *J Physiol* **590**, 21-31 (2012).
22. D. Jakob *et al.*, *J Mol Cell Cardiol* **158**, 49-62 (2021).
23. S. Thébault, F. Gachon, I. Lemasson, C. Devaux, J. M. Mesnard, *J Biol Chem* **275**, 4848-4857 (2000).
24. A. B. Byrne *et al.*, *Sci Transl Med* **14**, eabm4869 (2022).
25. M. Karlsson *et al.*, *Sci Adv* **7**, (2021).
26. R. Syeda *et al.*, *Elife* **4**, (2015).
27. C. M. Chen, N. Kraut, M. Groudine, H. Weintraub, *Cell* **86**, 731-741 (1996).
28. J. Wu *et al.*, *Cell Rep* **21**, 2357-2366 (2017).
29. M. Moroni, M. R. Servin-Vences, R. Fleischer, O. Sanchez-Carranza, G. R. Lewin, *Nat Commun* **9**, 1096 (2018).
30. E. Fotiou *et al.*, *Nat Commun* **6**, 8085 (2015).
31. K. Nonomura *et al.*, *Proc Natl Acad Sci U S A* **115**, 12817-12822 (2018).
32. Y. Xie *et al.*, *Scientific Reports* **6**, 28249 (2016).
33. A. Main, W. Fuller, *FEBS J* **289**, 861-882 (2022).
34. W. Zheng, E. O. Gracheva, S. N. Bagriantsev, *Elife* **8**, (2019).
35. X. Yang *et al.*, *Nature* **604**, 377-383 (2022).
36. P. Ridone *et al.*, *Journal of General Physiology*, (2020).
37. S. Ma *et al.*, *Science* **379**, 201-206 (2023).
38. J. Wang *et al.*, *Cell Reports* **38**, 110342 (2022).
39. C. Verkest, S. G. Lechner, *Current Opinion in Physiology* **31**, 100625 (2023).
40. L. Snider *et al.*, *Mol Cell Biol* **21**, 1866-1873 (2001).
41. J. Kazenwadel *et al.*, *J Clin Invest* **125**, 2979-2994 (2015).
42. A. Paix *et al.*, *Proc Natl Acad Sci U S A* **114**, E10745-e10754 (2017).
43. N. E. Sanjana, O. Shalem, F. Zhang, *Nature Methods* **11**, 783-784 (2014).
44. A. Punjani, J. L. Rubinstein, D. J. Fleet, M. A. Brubaker, *Nature Methods* **14**, 290-

296 (2017).
45. J. Zivanov *et al.*, *eLife* **7**, e42166 (2018).
46. E. F. Pettersen *et al.*, *Protein Sci* **30**, 70-82 (2021).
47. P. Emsley, K. Cowtan, *Acta Crystallogr D Biol Crystallogr* **60**, 2126-2132 (2004).
48. J. Jumper *et al.*, *Nature* **596**, 583-589 (2021).
49. P. D. Adams *et al.*, *Acta Crystallogr D Biol Crystallogr* **58**, 1948-1954 (2002).
50. S. Jo, T. Kim, V. G. Iyer, W. Im, *Journal of Computational Chemistry* **29**, 1859-1865 (2008).
51. S. Maurer-Stroh, F. Eisenhaber, *Genome Biology* **6**, R55 (2005).
52. J. Huang *et al.*, *Nature Methods* **14**, 71-73 (2017).
53. H. J. C. Berendsen, D. van der Spoel, R. van Drunen, *Computer Physics Communications* **91**, 43-56 (1995).
54. D. Van Der Spoel *et al.*, *Journal of Computational Chemistry* **26**, 1701-1718 (2005).
55. W. G. Hoover, *Physical Review A* **31**, 1695-1697 (1985).
56. S. Nosé, *Molecular Physics* **52**, 255-268 (1984).
57. M. Parrinello, A. Rahman, *Journal of Applied Physics* **52**, 7182-7190 (1981).
58. W. Humphrey, A. Dalke, K. Schulten, *Journal of Molecular Graphics* **14**, 33-38 (1996).
59. R. Gowers *et al.*, *MDAnalysis: a Python package for the rapid analysis of molecular dynamics simulations*. (2016).
60. N. Michaud-Agrawal, E. J. Denning, T. B. Woolf, O. Beckstein, *Journal of Computational Chemistry* **32**, 2319-2327 (2011).
61. W. Zheng *et al.*, *J Biol Chem* **291**, 25678-25691 (2016).
62. A. Percher *et al.*, *Proceedings of the National Academy of Sciences* **113**, 4302-4307 (2016).